REPORT DOCUMENTATION PAGE

Form Approved
OMB No. 0704-0188

1. REPORT DATE *(DD-MM-YYYY)*	**2. REPORT TYPE**	**3. DATES COVERED** *(From - To)*
05-05-2008	Final Performance Report	1 Jul 2004 – 31 Dec 2007

OPTICAL MEASUREMENTS OF AIR PLASMA

5a. CONTRACT NUMBER

5b. GRANT NUMBER
FA9550-04-1-0444

5c. PROGRAM ELEMENT NUMBER

6. AUTHOR(S)
Robert J Vidmar

5d. PROJECT NUMBER

5e. TASK NUMBER

5f. WORK UNIT NUMBER

7. PERFORMING ORGANIZATION NAME(S) AND ADDRESS(ES)

University of Nevada, Reno
Sponsored Projects, Mail Stop 325
1664 N Virginia Street
Reno, NV 89557-0240

8. PERFORMING ORGANIZATION REPORT NUMBER

9. SPONSORING / MONITORING AGENCY NAME(S) AND ADDRESS(ES)
AF Office of Scientific Research
4015 Wilson Blvd, Room 713
Arlington, VA 22203-1954

10. SPONSOR/MONITOR'S ACRONYM(S)
AFOSR/NE

11. SPONSOR/MONITOR'S REPORT NUMBER(S)

12. DISTRIBUTION / AVAILABILITY STATEMENT
UNLIMITED

13. SUPPLEMENTARY NOTES

14. ABSTRACT

Electron-beam impact ionization of air was studied in the context of optical diagnostics. The electron beam originates in a pulsed 100 keV 20-mA source and propagated through a 1/2 -mil aluminum transmission window into a 400-liter test cell. Plasma production in air was investigated over the pressure range of 636 Torr to 1 mTorr with pulse durations from 1 ms to 10 ms. Microwave diagnostics were used to quantify electron density and power; and an optical diagnostic was used to quantify ozone production. An additional effort to quantify byproducts of electron impact ionization, that are produced or consumed in the air plasma, resulted in preliminary results using laser-diode absorption spectroscopy to detect water vapor, carbon dioxide, and nitrous oxide. A transmission window and sensor to monitor the beam current was refined from a system that used a 1-mil aluminum foil to one with a ½-mil foil, which has greatly increased the beam current propagating through the foil into the test cell. This has improved the signal-to-noise-ratio for both the microwave and optical diagnostics.

15. SUBJECT TERMS
Air Chemistry, Air Plasma, Electron beam, Transmission Window, Optical Diagnostics, Ozone, Laser Diode

16. SECURITY CLASSIFICATION OF:			**17. LIMITATION OF ABSTRACT**	**18. NUMBER OF PAGES**	**19a. NAME OF RESPONSIBLE PERSON**
a. REPORT	**b. ABSTRACT**	**c. THIS PAGE**			Robert J Vidmar
UNCLASSIFIED	UNCLASSIFIED	UNCLASSIFIED	UNCLASSIFIED UNLIMITED	27	**19b. TELEPHONE NUMBER** *(include area code)* 775 682-9742

Final Performance Report *5 May 2008*

OPTICAL MEASUREMENTS OF AIR PLASMA

By: ROBERT J VIDMAR

Prepared for:

AIR FORCE OFFICE OF SCIENTIFIC RESEARCH
4015 WILSON BOULEVARD, ROOM 713
ARLINGTON, VA 22203-1954

CONTRACT NUMBER: FA9550-04-1-0444

University of Nevada, Reno
1664 North Virginia Street
Reno, Nevada 89557-0240 USA

ABSTRACT

Electron-beam impact ionization of air was studied in the context of optical diagnostics. The electron beam originates in a pulsed 100 keV 20-mA source and propagated through a 1/2 -mil aluminum transmission window into a 400-liter test cell. Plasma production in air was investigated over the pressure range of 636 Torr to 1 mTorr with pulse durations from 1 ms to 10 ms. Microwave diagnostics were used to quantify electron density and power; and an optical diagnostic was used to quantify ozone production. An additional effort to quantify byproducts of electron impact ionization, that are produced or consumed in the air plasma, resulted in preliminary results using laser-diode absorption spectroscopy to detect water vapor, carbon dioxide, and nitrous oxide. A transmission window and sensor to monitor the beam current was refined from a system that used a 1-mil aluminum foil to one with a ½-mil foil, which has greatly increased the beam current propagating through the foil into the test cell. This has improved the signal-to-noise-ratio for both the microwave and optical diagnostics.

CONTENTS

FIGURES

I INTRODUCTION

The goal of this effort is to investigate the power required to generate and sustain electron-beam generated air plasma using optical diagnostics. Plasma generated in air by means of an electron beam is highly efficient. Fast electrons propagating through air result in production of electron-ion pairs through the mechanism of impact ionization, which requires 33.7 eV per electron-ion pair. The air pressure, concentration of variable species, such as H_2O, the presence of an external electric field, and the electron temperature determine the deionization rate and power required for sustainment. The presence of an imposed electric field strongly influences the electron temperature, the deionization rate, and the generation of ionization byproducts, which under suitable conditions lowers the net power to generate and sustain plasma. The air chemistry that governs the deionization process is complex and requires a full simulation of all relevant species and reactions to predict the deionization process. To improve the database for modeling deionization, optical diagnostics are used to quantify the power as well as the air-chemistry of individual species. It is possible to measure both the concentration and the growth or decay rate of a species, such as ozone, to determine if the air-chemistry model properly represents all relevant reaction channels.

A 100-keV electron source produces air plasma in a test cell equipped with RF and optical diagnostics. These diagnostics quantify the electron density as a function of time as well as associated species that bear on the overall deionization air chemistry. Optical diagnostics provide a non-perturbing method to quantify species, such as O_3, CO_2, H_2O, and N_2O. A high-energy electron beam produces plasma, where the electron temperature is generally higher than the bulk gas temperature and is not in equilibrium with the vibrational temperatures of nitrogen or oxygen, and is considered to be in nonequilibrium. Such plasma have been investigated by Macheret *et al* (2001) for ambient air at 700 K, Adamovich (2001) for optically pumped $CO/Ar/O_2$ and $CO/Ar/N_2$ mixtures at 700 K, Yu *et al* (2002) for air at 2,000 K, and Stark and Schoenbach (2001) for air at 2,000 K. The results consistently show that a nonequilibrium plasma requires less power than one in equilibrium. The work conducted bears on the properties of a transient nonequilibrium plasma.

Medical and aerospace applications benefit from better knowledge relating to the generation of air plasma with a high-energy electron beam. Medical applications include large volume bio-decontamination, coatings for implants, and plasma surgery. Aerospace applications include hydrodynamic flow control, mitigation of supersonic shock waves, plasma assisted combustion for aircraft and hypersonic engines, RF effects, and agile plasma mirrors for radar systems. The deionization chemistry required by these application cover the range of electron densities from 10^{10} to 10^{13} electrons/cm^3 and span pressures from 760 Torr at sea level to 1 mTorr at 300,000 ft.

II TECHNICAL APPROACH

A. Facility

The University of Nevada, Reno, air-plasma facility consists of an air-plasma test cell, a 100-keV electron-beam source, and several real-time diagnostics. This facility is described in reports Vidmar et al (2005, 2006, and 2008). The electron-beam system in Fig 1 from Kimball Physics consists of an EGH-8201 Electron Gun and EGPS-8201 power supply. The unit originally produced an electron beam ported to the test cell through a 25.4-μm aluminum transmission window. A problem soon developed relating to the measurement of beam current impinging on the transmission window, since a fast acting current monitor was not supplied with the electron beam source. An insulating structure made from Teflon was used to insulate the transmission window from the ground plane and provide an indication of beam current. The absolute calibration of beam current was difficult because plasma generated within the test cell in Figure 2 provides additional current paths to ground. A thin metal mesh was subsequently introduced between the transmission window and the electron source. This provided a clean measurement of beam current.

Figure 1. Electron source and test cell.

The beam current, however, was systematically degrading below the manufacturers specification. The low beam current was traced to a virtual leak associated with the Teflon insulator used to isolate the transmission window from the ground plane. This virtual leak produced gas that flowed up the transit tube from the top of the test cell to the high voltage acceleration region of the electron beam source. The gas flowed through the exit orifice of the source through the high-voltage acceleration region of the source then onto the cathode. The pressure was a least a factor of 10 higher than the pressure reading for the electron source.

These issues were remedied by replacing the Teflon insulator with an all metal system, and the short nipple, visible in Fig. 1, at the bottom of the electron gun that connects the gun to the test cell was replaced with a custom 5-way cross. An additional turbo pump and vacuum gauge were installed to the 5-way cross. The electron source now operates at a pressure in the low 10^{-9} Torr

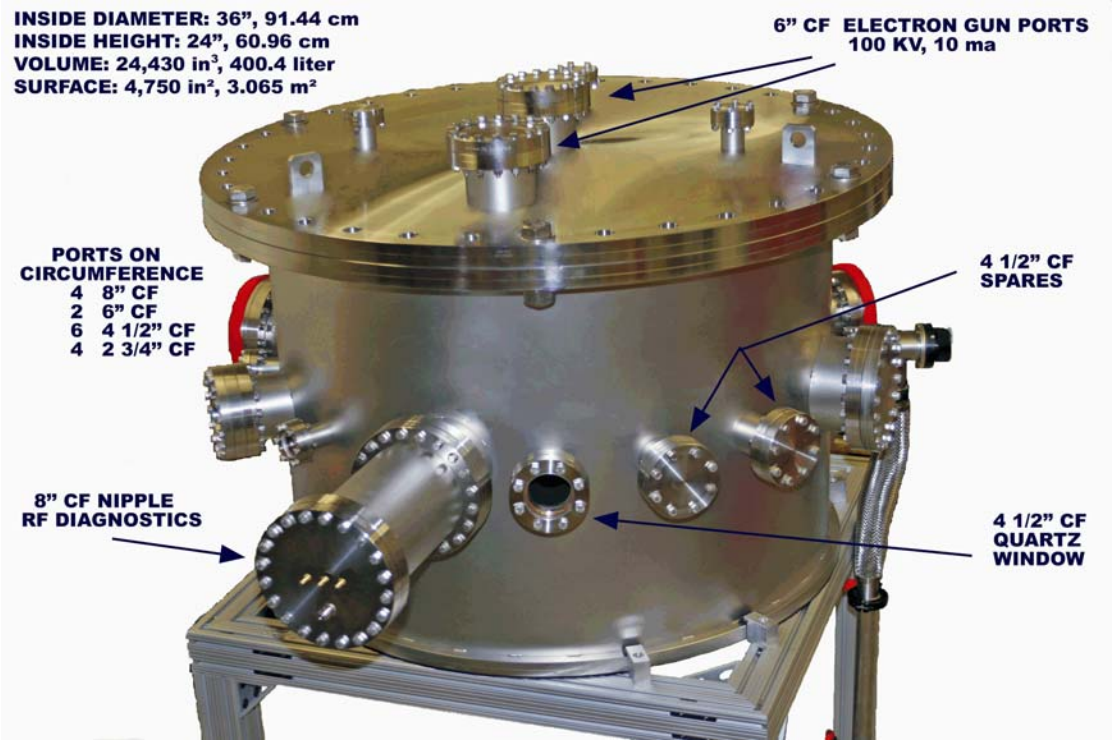

Figure 2. Test cell with specifications.

range. The pressure associated with the differential pumping above the transmission window is approximately four times greater than that in the electron gun, due to the much larger surface area exposed to vacuum. Beam quality improved and the pumpdown time for the electron gun changed from a minimum of 3 days to 1 day.

The test cell in Fig. 2 was configured to support rf diagnostics through two 8" CF ports with rf horns mounted in 8" nipples. Specifically, quadrature detection at 10 GHz with a propagation path directly through the test cell is used to obtain magnitude and phase information, simultaneously. Electrical connections to the mesh sensor and graphite plates within the test cell are made through 2 ¾" CF ports on the top and bottom of the test cell. One port on the circumference supports a variable leak for backfilling the test cell with air or other gases, a second port is allocated for pressure measurements with the remaining ports open for optical diagnostics. An ozone sensor mounts to one port and components for laser-absorption spectroscopy occupy four additional ports. These ports provide diagnostics on a center plane 12" from the lower surface of the upper flange in Fig. 2. The distance from the electron-beam transmission window foil to the optical plane is approximately 10" or 25.4 cm.

B. Transmission Window and Mesh Sensor

The transmission window and current sensor described above was replaced with an all metal system using ceramic insulators to maintain electrical isolation. The complete system depicted in Fig. 3 shows a 60 mm inside diameter copper ring that limits the maximum beam diameter through the system. The beam propagates through a mesh current sensor and honeycomb support. Both the mesh sensor and honeycomb

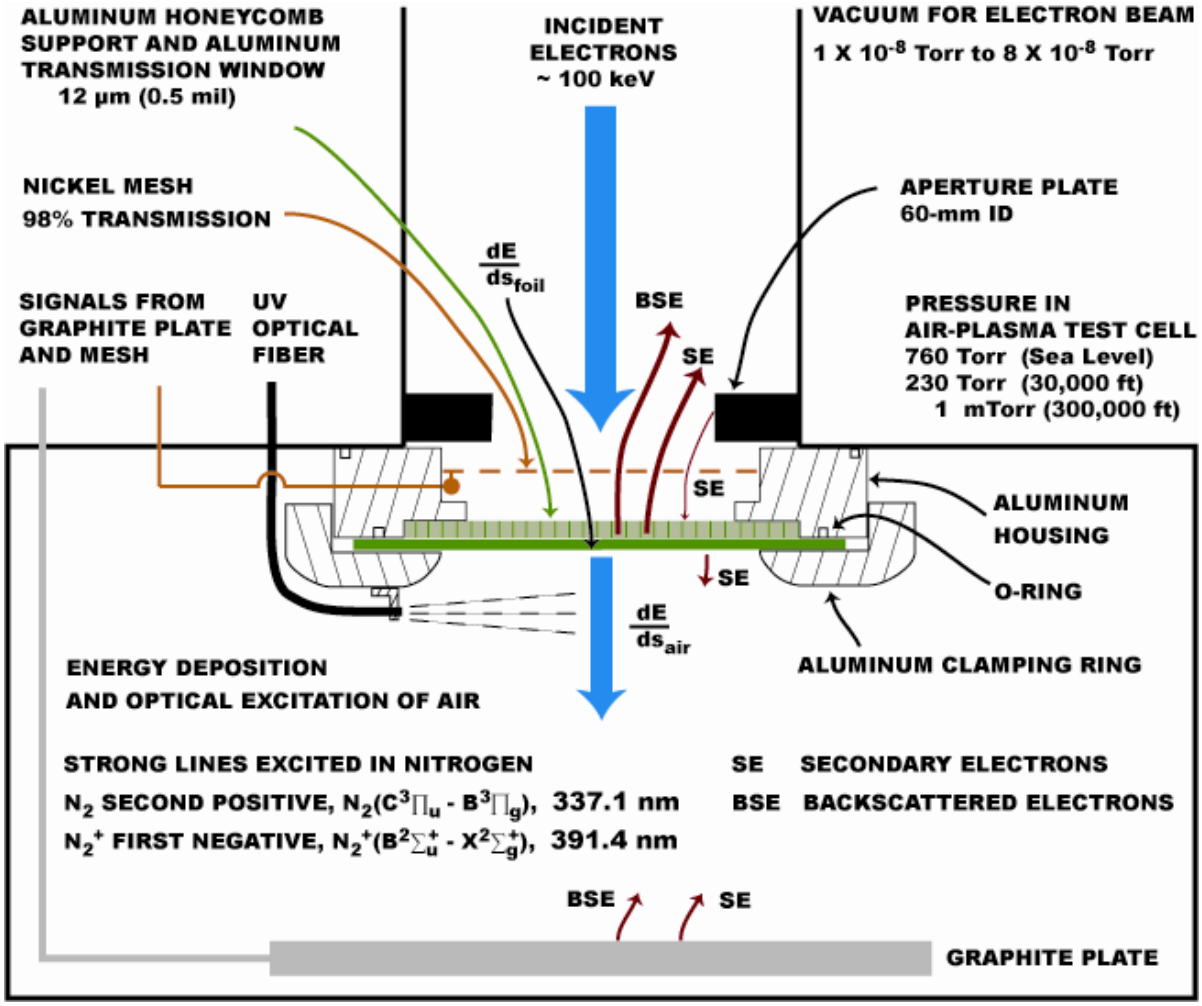

Figure 3. Transmission window and current and optical sensors.

support are mounted in an aluminum housing with two O-ring seals. A transmission window foil is centered on the honeycomb support. An aluminum-clamping ring at the bottom of Fig. 4 compresses both O-rings and seals the system to the upper flange of the test cell. The six bolts used to fasten the assembly to the upper flange were removed but their Teflon insulators remain visible. The surface of the clamping ring, not visible in Fig. 4, was fitted with a SMA connector for optical measurements. The optical fiber has an axis parallel to the foil and approximately 18.9 mm from the foil surface.

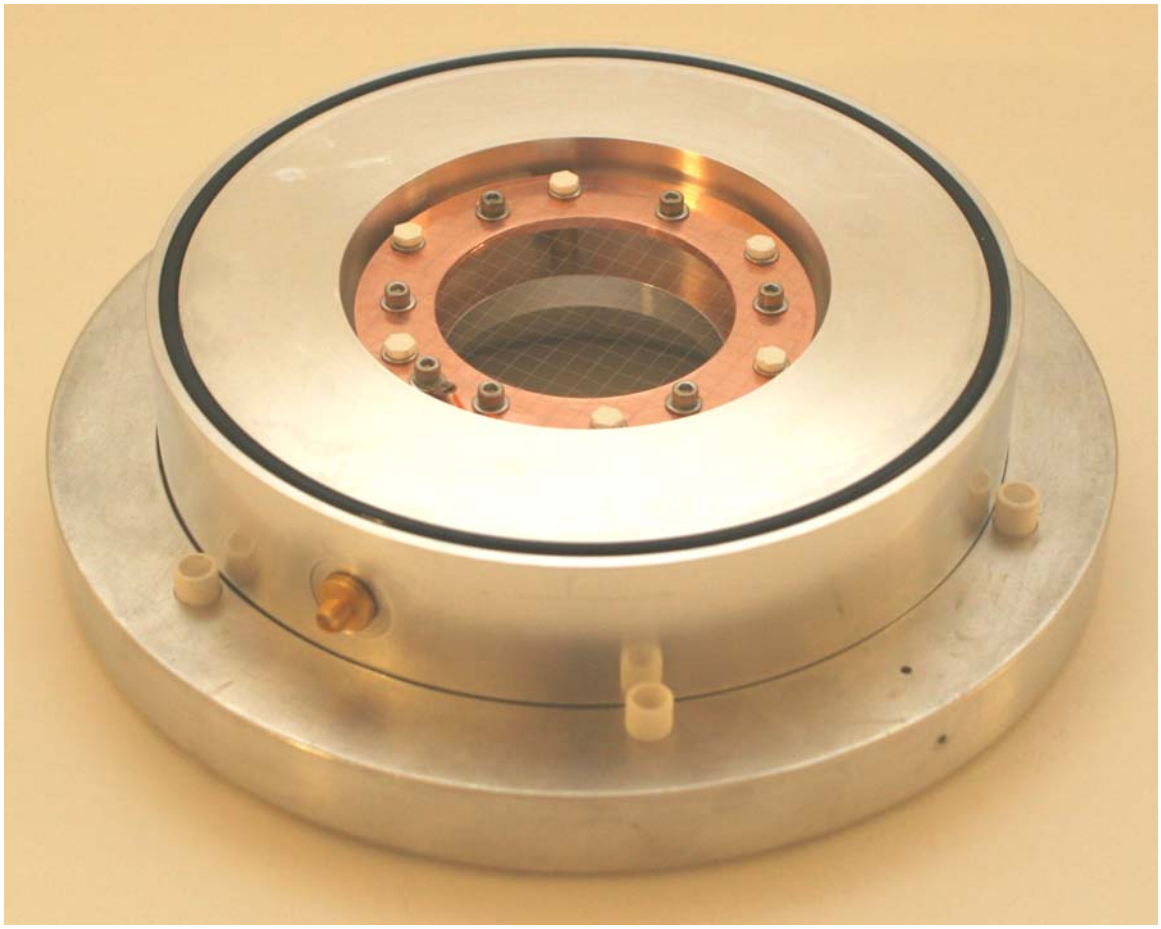

Figure 4. Mesh sensor mounted in aluminum ring with SMA feed through.

The beam propagates through a 2-mil nickel mesh with 98% transparency and is mounted on a copper disk as shown in Fig. 4. Ceramic standoffs and ceramic screws fasten the mesh assembly to the aluminum housing. The electrical signal from the mesh connects to a SMA vacuum bulkhead connector through the side of the aluminum housing. The small SMA connector shown in Fig. 4 has been replaced with a larger connector that seals more aggressively to the aluminum housing. The electrical signal from the mesh connects to a DSO with a 52,630 Ω composition resistor in parallel to a 1-MΩ DSO inpu. The resulting calibration for the mesh sensor is 1 mA/V.

The honeycomb support shown in Fig. 5 has evolved during the course of this project. The initial support was a round disk of honeycomb material placed in a recess in an aluminum flange. This initially worked for a short time but atmospheric loading produced stresses in the honeycomb joints that resulted in seam failures, bowing of the honeycomb, and eventual failure. Several thicknesses of honeycomb were tried with 10-mm thick providing the best result, which still had a tendency to failure and bowing. Application of vacuum epoxy to the perimeter of the honeycomb disk provided additional rigidity to the disk. The additional stiffness eliminated the bowing and provided stable operation over

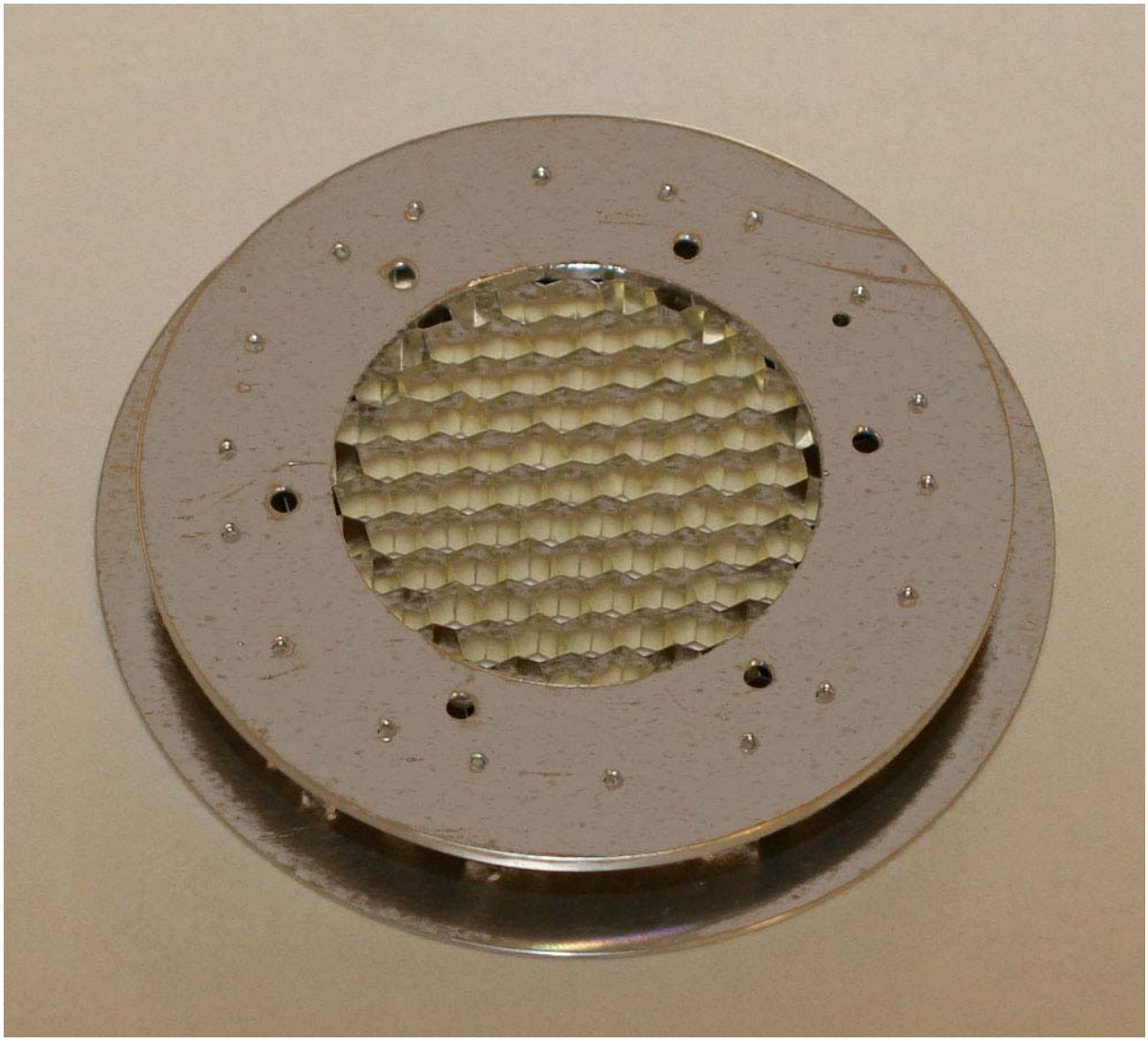

Figure 5. Honeycomb assembly with double rings screwed together.

months of atmospheric pressure loading. This epoxy had a low outgassing coefficient, but it in addition to the outgassing of the Teflon insulator proved to interfere with high current operation of the electron source.

To over come the outgassing issue an all-metal system was developed. Prior experience with the 10-mm honeycomb suggested that a fixed boundary condition was necessary to stiffen an unsupported 10-mm honeycomb for long term use. A box-beam consecution provides a fixed boundary, and was adopted for use in the form of two annular plates with the honeycomb sandwiched between; see Fig. 5. The upper plate interfaced with the foil and has a beveled edge, not visible in Fig. 5.. The lower plate, visible in Fig. 5, shows the assembly and the 18 threaded holes for fasteners. It was impossible to use a standard 18-hole layout because the particular honeycomb pattern did not naturally match-up

with that screw hole pattern. A custom screw-hole pattern based on AL002720 honeycomb obtained from Goodfellow Corporation was developed. This honeycomb has an average density of 0.083 g/cm3, is made of 5052 aluminum, and uses phenolic resin to form the honeycomb. The six through holes visible in Fig. 5 were for attachment to a fixture used during fabrication.

A close-up topside view of the honeycomb with a transmission-window foil appears in Fig. 6. Common aluminum foil, such as 1100-O in ¾-mil and ½-mil thickness with yield strength of 35 MPa, is unsatisfactory, because it yields under stress, thins, and produced copious pinholes during initial pumpdown. Use of 1-mil foil was successful but beam degradation through 1-mil foil is high. Aluminum foils were researched and a number of high yield strength foils identified. The

Figure 6. Initial atmospheric loading of 12.7-μm thick 1145/12355-H19 aluminum foil.

foil used in Fig. 6 is ½-mil (12.7 μm) aluminum alloy1145/12355-H19, which has yield strength of 145 MPa. This high tensile-strength foil on the 6.3 mm cell size of the honeycomb was stable and did not produce any unusual stress points that ruptured under atmospheric pressure loading.

The initial atmospheric pressure loading test shown in Fig. 6, however, resulted in several pinhole leaks. These leaks occurred in conjunction with flat head screws that produced stress points, because the screws were not sufficiently countersunk. Additional stress points were associated with the entire honeycomb sandwich extending a few mils too high in its recess in the aluminum housing. A knife-edge stress developed around the outside diameter of the upper disk caused by the clamping ring. The smooth transition to a 20-mil step down to the honeycomb on the inside diameter of the upper flange is evident in Fig. 6 and did not produce any pinhole leaks. Large grains of sand/dust under the foil in this transition region, however, did produce pinholes. The assembly was retouched so all screw holes lied flush on the surface, the aluminum-housing recess was lowered so the entire assembly lied flush under the clamping ring. On the subsequent test, all particles on the foil and honeycomb assembly were removed by dusting with canned pure dry air prior to final assembly. The second test foil has survived 20 days of atmospheric pressure loading, two pumpdown cycles with one month of downtime between cycles. On the last day of use, the pressure directly above the foil, honeycomb, mesh, and aluminum housing was 2.75×10^{-8} Torr and the electron source operated at 2.95×10^{-9} Torr.

The all metal honeycomb support, mesh sensor, and differential pumping are necessary for the high current operation of the electron source. The source on occasions produced 20 mA prior to the introduction of the first Teflon ring to provide a beam-current measurement. The 20 mA beam current was observed using a graphite plate collector at the bottom of the tank with the Teflon ring removed for axial alignment and focusing. Subsequent measurements with the all-metal system and a filament and grid assembly that was inadvertently overheated and exposed to high-pressure air produced about 5.5 mA for several weeks of operation. A new filament and grid would improve the maximum beam current as well as reducing the first anode spacing to the grid to increase the extraction electric field. The current anode spacing is too wide as beam current keeps increasing as the anode voltage increases to its maximum. Adjustment of the anode spacing requires several weeks, so the current anode spacing is being used until the installed filament fails. The results reported in Vidmar *et al* (2008) used the al-metal system and a ½ mil foil.

C. Nitrogen Emissions.

The SMA bulhead adapter, shown in Fig. 6, was connected to an Ocean Optics, Model HR2000+ multichannel diode-array detector by a 600 μm diameter optical fiber. The HR2000+ requires a minimum of 1 ms to acquire a full spectrum from 240 nm to 700 nm. Both tungsten and deuterium lamps were used to calibrate the spectrometer response. The strongest lines emitted were the N_2 Second Positive system and the N_2^+ First Negative system, as shown in Fig. 7, which was obtained in a single 5-ms shot.

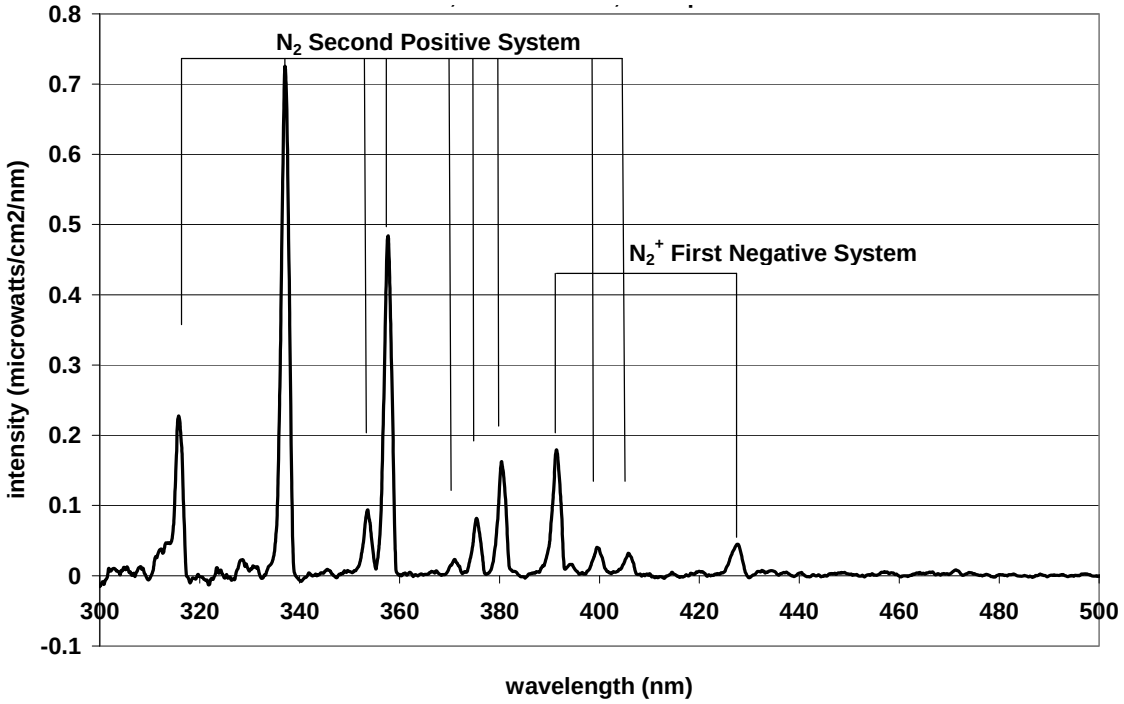

Figure 7. Nitrogen emissions, calibrated, 100 keV, 21 Torr lab air, 5 ms pulse.

These emissions were quantified as a step towards using an optical fiber as an optical Faraday cup. It is known that the optical intensity of nitrogen emissions is proportional to beam current and is linear with pressure up to 15 Torr. By systematically quantifying the 337.1-nm emission as a function of current and pressure in Fig. 8 and 9, the effects of excited state quenching are folded into the calibration curve. Fig. 8 quantifies the 337.1 nm line as a function of beam current at 600 Torr. The effect of quenching as a function of pressure is quantified in Fig. 9. By taking measurements near the foil, where the electron-beam current density can be estimated using MAGIC, Vidmar and Stalder (2007), the optical fiber is calibrated. The optical fiber or one identical to it can be moved to other locations in the test cell. The ratio of the count rate at the new location to that near the foil and a correction for the beam energy and energy deposition rate at the new location from MAGIC provides an estimate of the electron-beam current density at the new location. This will be useful in quantifying the spatial electron beam current distribution on the optical plane.

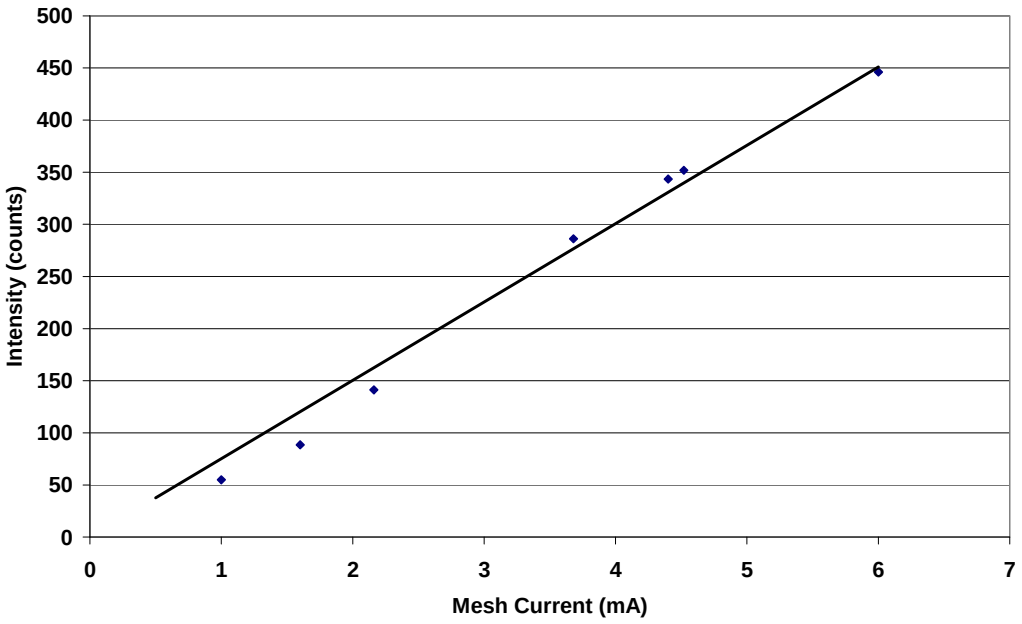

Figure 8. Second Positive emission at 337.1 nm versus beam current incident on foil.

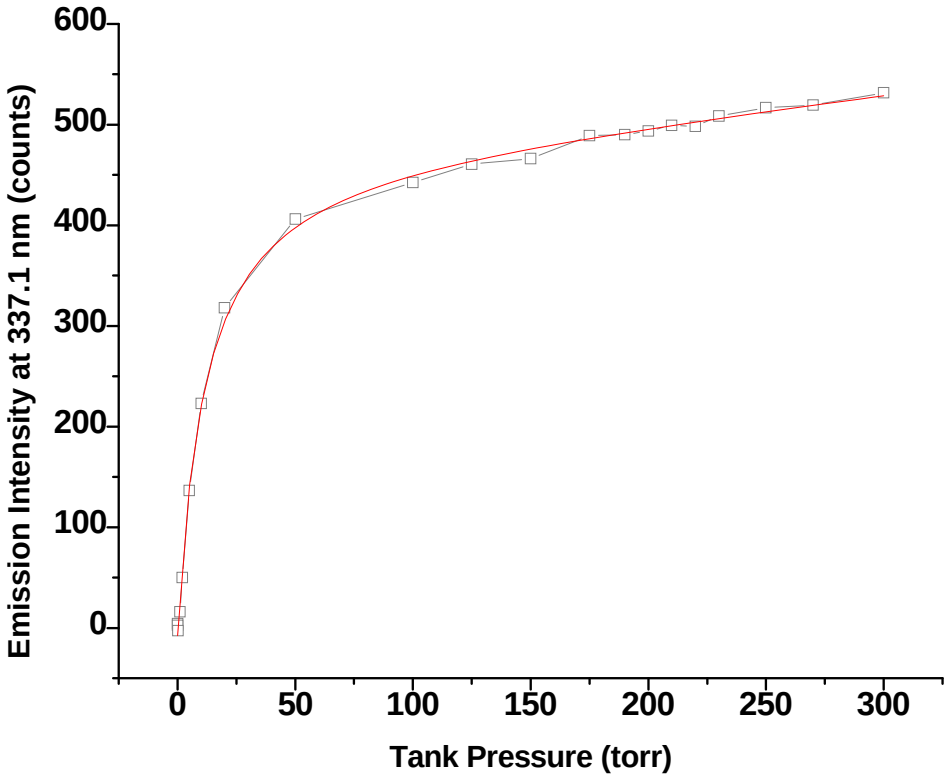

Figure 9. Second Positive emission at 337.1 nm versus air pressure. The smooth curve is a least squares fit.

D. Ozone Detection.

Ozone is produced in the air plasma test cell by the electron beam. The amount of ozone was estimated for a pressure of 225 Torr (equivalent to an altitude of 30,000 ft) using an air-chemistry code. A concentration that linearly ramps up to 1.6×10^{13} cm^{-3} was estimated for beam operation at 100 keV and 5.5 mA. This concentration is high enough for detection using a White cell, shown in Fig. 10. The mirrors form a multi-pass cell, so that light from the LED source crosses the midplane multiple times. The system has undergone many refinements. Currently, the source is a UV LED from Sensor Electronic Technology Inc., UV-TOP®250TO39HS. Light from the UV source enters the test cell through a quartz window. Light from the test cell is coupled through an optical fiber to a Hamamatsu Model H5783-03 micro-photomultiplier tube that incorporates a narrow band filter centered on 254 nm. The center wavelength for this filter is on the peak of the absorption cross section for ozone. The single pass absorption for a path length of 50 cm in the test cell is about 6%. A ten-pass system is in operation with an effective path length of 500 cm.

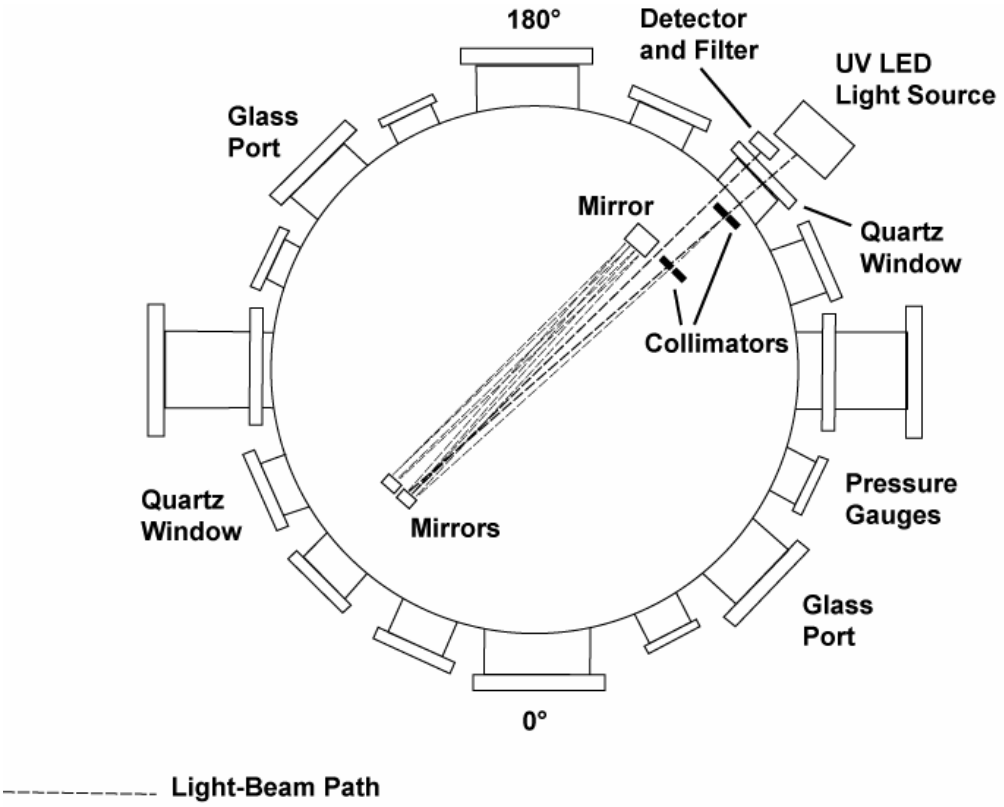

Figure 10. White cell mounted in air-plasma test cell with UVLED source.

A series of experiments were conducted with the electron beam operating at 100 keV, 5.6 mA, and 10-ms duration to quantify ozone production as a function of pressure and to quantify the temporal production of ozone during an

electron beam pulse. The variation of ozone production with pressure appears in Fig. 11.

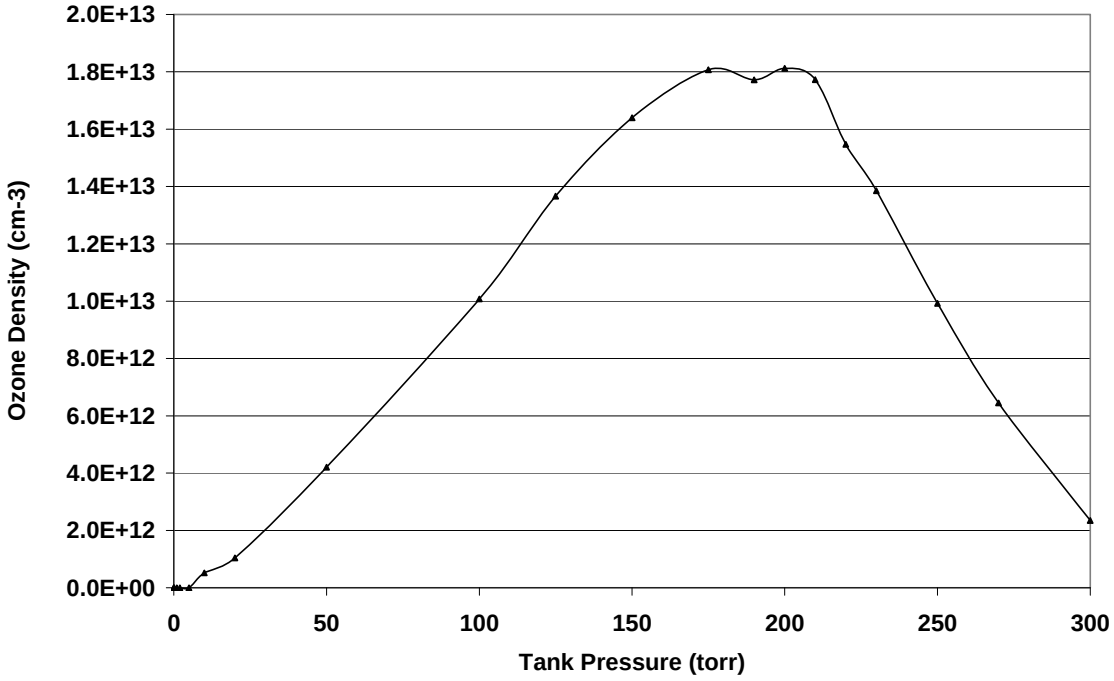

Figure 11. Chord averaged ozone concentration measured on the test cell Centerline with a White cell. Electron beam operated at 100 keV, 5.5 mA, and 10-ms duration onto the transmission window foil.

From low pressure to approximately 200 Torr the concentration increases as the concentrations of both O_2 and O increase. Above 200 Torr the concentration decreases as the electron beam range becomes increasingly too short to reach the optical plane. Modeling with MAGIC quantifies the decrease in range as well as standard tables for electron range in air.

The temporal evolution of ozone predicted by an air-chemistry code was for a linear increase in ozone as a function of time. The time evolution of the raw ozone signal from the detector shown in Fig. 12 demonstrates a sudden onset with 10 ms of decreasing signal amplitude. Noise masks some of the signal but the trend is linear absorption with time. The decrease in signal may originate from ozone produced near the foil diffusing into the test plane. To account for that possibility, a longer time scale for a single shot was used and the signal in Fig. 12 was obtained. This figure shows the prompt ozone absorption followed by diffusion out of the center plane in 2-3 s. Consequently, the ozone detected is primarily that which is generated promptly on the optical plane. Because ozone can have a lifetime of ~1,000 s in a stainless steel tank, it is important to pump down the test cell frequently to eliminate the buildup of ozone over time.

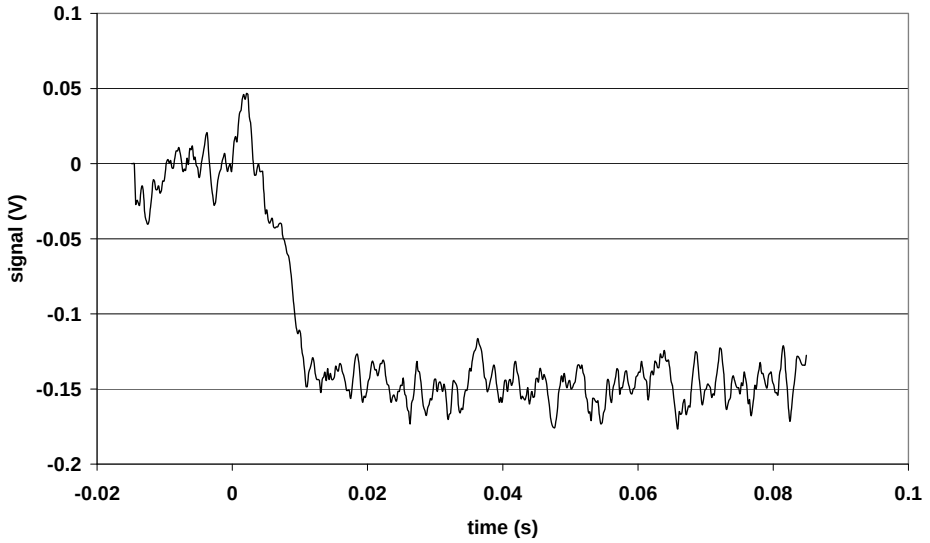

Figure 12. Absorbance signal for prompt ozone production at 200 Torr in lab air with 5-point average. Electron beam operated at 100 keV, 5.5 mA, and 10-ms duration onto the transmission window foil.

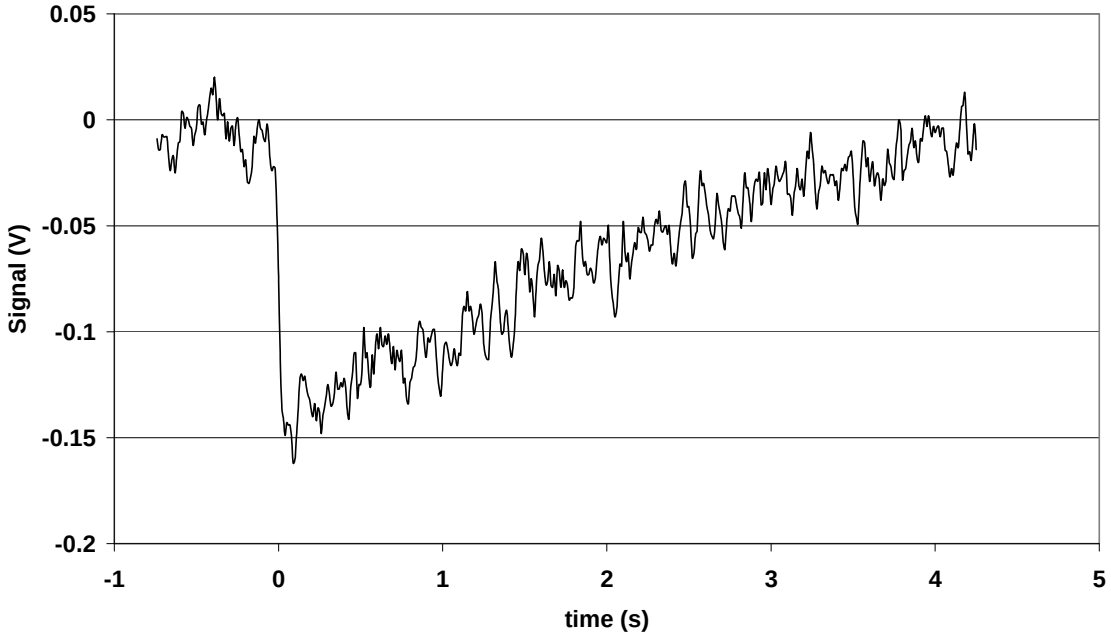

Figure 13. Prompt ozone production followed by diffusion out of measurement plane at 200 Torr. Electron beam operated at 100 keV, 5.5 mA, and 10-ms duration onto the transmission window foil.

E. Laser Diode Absorption Spectroscopy.

Absorption techniques based on infrared radiation from tunable diode lasers provide a means to detect many diatomic and polyatomic species. Because our time scales are in the 1 ms to 10 ms range, there is a strong possibility of obtaining real-time absorption data of species of interest. The species of immediate interest are H_2O and CO_2, because they are present in the test cell with variable concentrations. H_2O for example is absorbed on the test cell surfaces at high pressure and desorbs at lower pressures. Measurements of H2O concentration prior to and after an electron beam pulse are approximate. An in situ measurement during a beam pulse removes all uncertainty. Other species, produced by the electron beam in air, are CO, CO_2, NO and N_2O. The 4-channel ILX Lightwave system and laser diodes shown in Fig. 14 are the principal components of the absorption spectroscopy system. This equipment, assorted mounts, windows, lenses, and alignment hardware in Fig. 15 produced the sample spectrum in the upper left of Fig. 15..

Figure 14. ILX Lightwave LDC-3900 4-channel controller, LCM-39427 control modules, LDM-4984 butterfly mount; NEL America NLK1E5GAAA 1392-nm laser diode for H_2O, NLK1L5GAAA 1581-nm laser diode for CO and CO2, KELD1F5DAAA 1790-nm laser diode for NO; Thor Labs PDA10CS 700-1800 nm InGaAs detector.

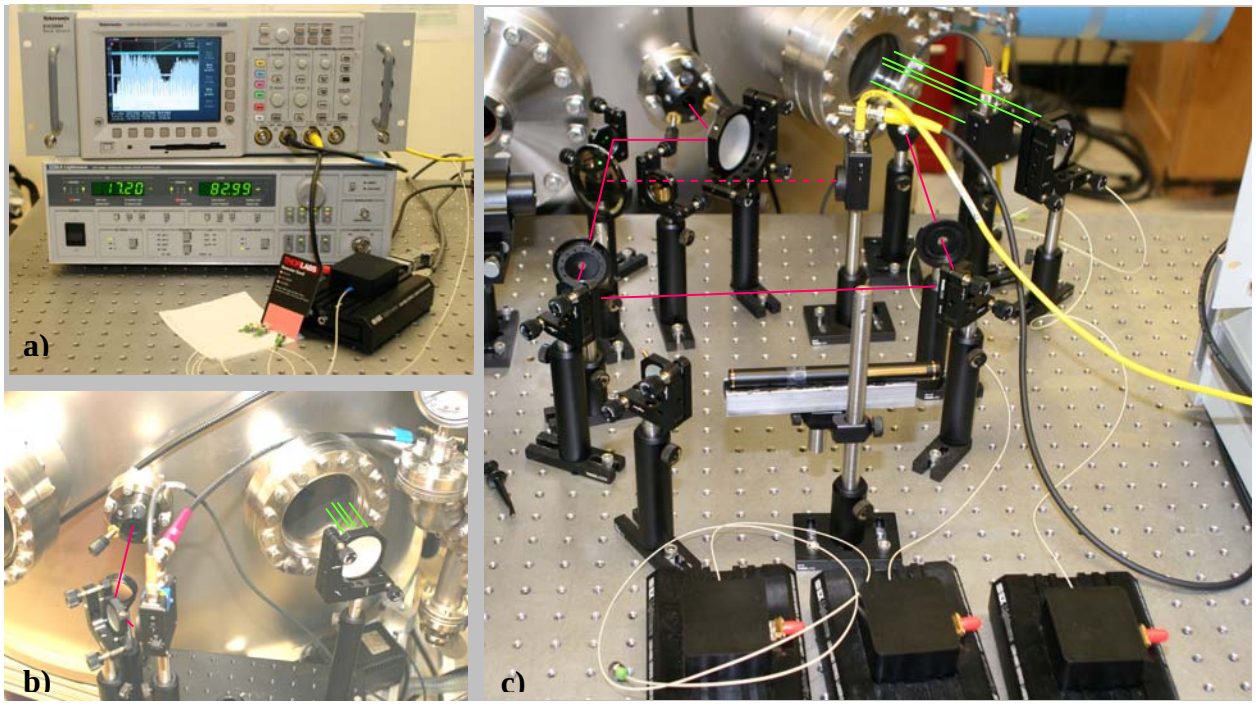

Figure 15. Laser absorption spectroscopy hardware. a) ILX system with sample spectra displayed on DSO. b) Detector mounted on across test cell in multipass configuration. c) Laser diodes, high finesse mirrors, and alignment optics.

The equipment in Figs. 14. and 15 was configured for use based on several detection schemes. The techniques investigated were cavity ringdown spectroscopy (CRDS), Paul *et al* (2001), integrated cavity off-axis spectroscopy (ICOS) Paul *et al* (2001) and Kluczynski and Axner (1999); single pass and multipass systems, and second-harmonic (2f) detection, Kluczynski and Axner (1999). CRDS while extremely sensitive requires low noise laser diodes and a tank free of vibrations and flexing under pressure cycling. The ICOS approach is better suited for the air-plasma experiments and an on-axis feed to high finesse mirrors produced a long path length for absorption. The 2f approach applied to water vapor works well.

1) One-to-Four Pass Water-Vapor Detection. Water vapor has a strong absorption line around 1390 nm and was detected using a one-to-four pass system in laboratory air depending on pressure. Observations were made down to 1 Torr using a single pass through the test cell as shown in Fig. 16. The time resolution for this high signal-to-noise ratio line was approximately 1 ms. The absorption signal depends on the water vapor concentration in the test cell and the water vapor adsorbed to the inner surface of the test cell. Absorption lines persisted after a short exposure to lab air with subsequent pumping down to a few mTorr. Water vapor out gassed from the inner surface of the test cell. Under electron beam bombardment, water vapor dissociates and its concentration diminishes a few percent. The concentration does not recover to its preshot

magnitude, so the dissociation products recombine to form other species. For air pressures below 1 Torr, two high reflective (HR) mirrors with *R*=99.9985% at 1390 nm formed a high finesse cavity across the test cell with a 1-m single pass distance.

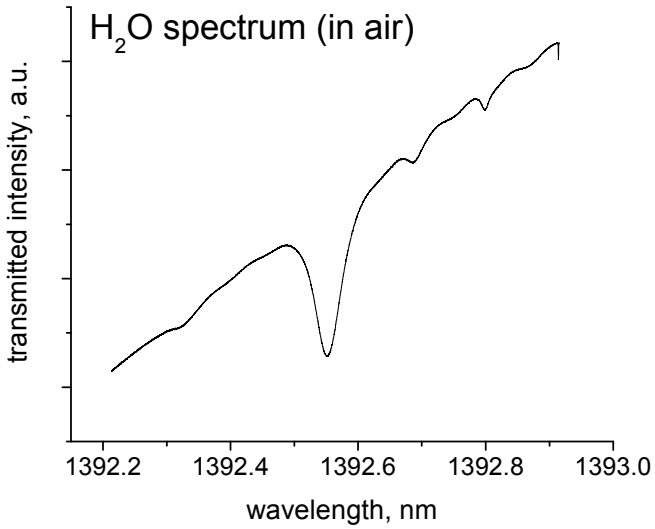

Figure 16. Detection of water vapor near 1392.5 nm in 80Torr lab air.

2) High Finesse Cavity for N_2O, H_2O, and CO_2 Detection. Although cavity ringdown was attempted, it proved to be too difficult to stabilize in the test cell operational environment. A high-finesse cavity absorption approach proved to be more successful. Cavity modes for the mirror separation in the test cell have a spacing of $d\ell \sim 6 \times 10^{-4}$ nm. For H_2O the Doppler FWHM at room temperature is $\delta\nu = 5 \times 10^{-3}$ nm, which is much larger, and permits observation using the envelope mode of a DSO for signal processing, as shown in Fig. 17 for N_2O. Envelope mode produces a gain of signal-to-noise ratio but decreases the temporal resolution.

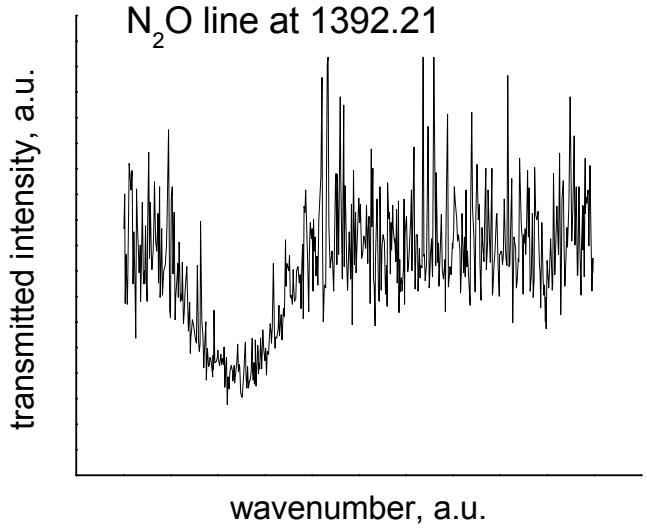

Figure 17. Envelope mode DSO processing of N_2O absorption near 1392 nm.

Using N_2O from a gas cylinder to fill the test cell, measurements of absorption greater than 40% and concentrations of N_2O down to10^{16} cm^{-3} were observed as shown in Figs. 17 and 18. The absorption path length for N_2O is approximately 3.3 km, which implies 3,300 passes through the test cell. An experiment with 15 Torr N_2O with 4 Torr of lab air produces both N_2O and H_2O lines, simultaneously, near 1392 nm, as shown in Fig. 18. The feature on the right lower side of Fig. 18 is the N_2O line with the broad water absorption line at 1392.53 nm to its left. Figure 19 is an example of N_2O detection in 636 Torr of laboratory air. The thick curved bar in Fig. 19 identifies collisional broadening centered at 1391.18 nm.

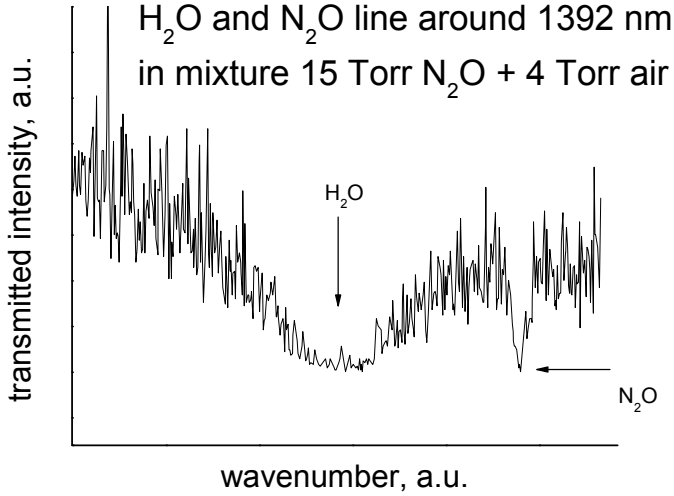

Figure 18. Envelope mode detection of H_2O and N_2O absorption around 1392 nm.

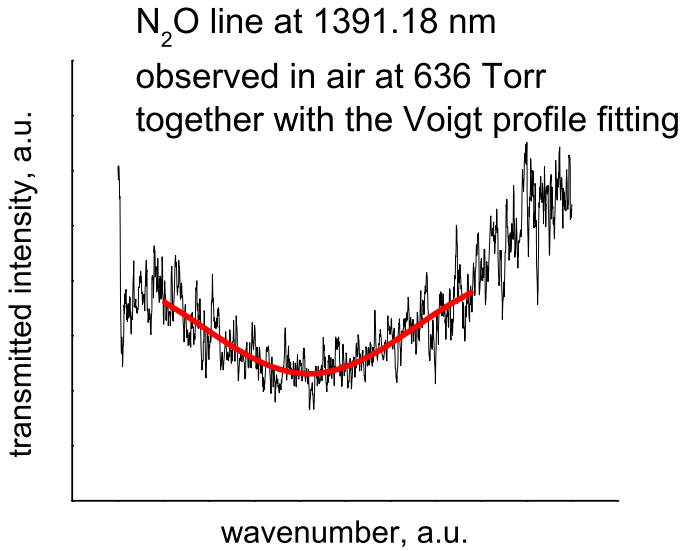

Figure 19. Detection of N_2O in 636 Torr of laboratory air. The thick bar is a fit to a Voigt collisional broadening profile.

The absorption lines of CO_2 near 1580 nm were observed using HR mirrors designed for peak reflectivity at 1390 nm. The detection of CO_2 at 1579.57 nm exhibited a reasonable signal-to-noise ratio and was detectable in laboratory air from 636 Torr down to 40 Torr. An example of detection in 40 Torr air is shown in Fig. 20. Because the reflectivity of the 1390 nm HR mirrors is much lower at 1580 nm, the cavity modes are more widely spaced and the system was easy to stabilize. The CO line that is nearby was not detected because the multi-bounce absorption path was not long enough with the mirrors utilized. Alignment of the mirrors for these experiments used radiation at 1790 nm, where the 1390-nm HR mirrors are nearly transparent.

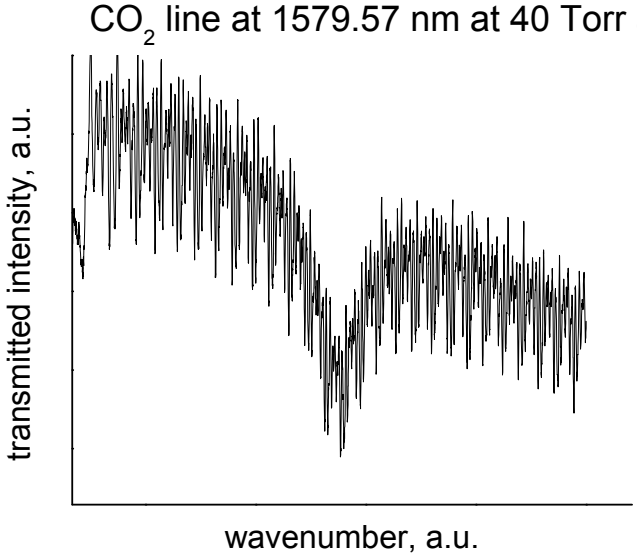

Figure 20. Detection of naturally occurring CO_2 in 40-Torr laboratory air.

An improvement in the current signal-to-noise ratio made possible by stabilization of the cavity modes would permit a time resolution for measurements of 1 ms. That resolution would permit detection of the OH radical at 1391.52 nm. A sensitivity of 10^{13} cm^{-3} may be possible with the current hardware. Based on air-chemistry code predictions an electron beam could produce a concentration of 10^{15} cm^{-3} OH at 760 Torr. This should fall within the range of detection for future experiments. Other high finesse cavities at 1580 nm and 1790 nm would increase sensitivity for detection of NO and CO.

III RESULTS

The major research results derived from this effort are the following:

- A current monitoring system and 12.7-μm transmission window with differential pumping improved the utility of the 100-keV electron source.

- Detection of ozone has progressed to a reliable second-generation design and is providing real-time concentration measurements in conjunction with other diagnostics.

- Detection of nitrogen emissions at 337.1-nm as a function of pressure provides an indirect measurement of beam current.

- Initial setup of laser diode absorption spectroscopy for real-time water-vapor concentration measurements.

- Real-time measurements of electron density, ozone concentration, and power as a function of pressure reported in Vidmar *et al* (2008).

IV PERSONNEL, INTERACTIONS, AND PUBLICATIONS

Personnel. The personnel for this effort consisted of three primary researches, students, and support staff as noted below.

Primary Personnel

- Robert J Vidmar, Principal Investigator
- Kenneth R Stalder, Consultant
- Anna Y Serdyuchenko, Post Doctoral Scholar

Students and Technical Support

- Megan V. Seeley, Graduate Student Physics
- Quinn J Sinnott, Student Physics
- Andrew X Oxner, Laboratory Technician

Interactions. Research conducted on this project was presented at the 57th, 58th, 59th and 60th Gaseous Electronic Conferences, and at the 43rd, 44th , and 46th Aerospace Sciences Meeting and Exhibit American Institute of Aeronautics and Astronautics Conference in Reno Nevada, the 33rd International Conference on Plasma Science, and the 2007 Pulsed Power and Plasma Science Conference. There were numerous interactions at these conferences with representatives from DoD Laboratories, National Laboratories, private companies, and Universities from around the world.

Publications Supported by AFOSR Grant Number FA9550-1-0015

Stalder, K, Vidmar, R., Nersisyan, G., and W. Graham, "Modeling the Kinetics in High-Pressure Glow Discharges," PT2.059, 57th Annual Gaseous Electronics Conference, 26-29 Sept, Shannon, The Republic of Ireland, GEC04, 2004, Bulletin of the American Physical Society, 2004.

Vidmar, R. J., and K. R. Stalder, “Air-Plasma Experimentation at the University of Nevada, Reno,” AIAA 2005-0791, p 12, Jan, 2005.

Vidmar, R. J., K. R. Stalder, and M. V. Seeley “Electron Beam Produced Atmospheric Pressure Air Plasma: Measurements of Electron Density and Optical Observations,” AIAA 2006-791, p 10, Jan, 2006.

Stalder, K. R., R. J. Vidmar, G. Nersisyan, and W. G. Graham, “Modeling the Chemical Kinetics of High-Pressure Glow Discharges in Mixtures of Helium with Real Air," Journal of Applied Physics, Vol 99, No 9, pp 93301-1-8, 1 May 2006.

Vidmar, R. J., M. V. Seeley, A. Y. Serdyuchenko, and K. R. Stalder, “Electrical, RF, and Optical Diagnostics in E-Beam Excited Air,” AIAA 2008-1111, p 17, Jan, 2008.

Presentations Supported by AFOSR Grant Number FA9550-1-0015

Stalder, K, Vidmar, R., Nersisyan, G., and W. Graham, "Modeling the Kinetics in High-Pressure Glow Discharges," PT2.059, 57th Annual Gaseous Electronics Conference, 26-29 Sept, Shannon, The Republic of Ireland, GEC04, 2004, Bulletin of the American Physical Society, 2004.

Vidmar, R. J., and K. R. Stalder, “Air-Plasma Experimentation at the University of Nevada, Reno,” Session 111-WIG-5, AIAA 2005-0791, p 12, 43rd Aerospace Sciences Meeting and Exhibit, Reno, NV, 10-13 Jan, 2005.

Vidmar, R., K. Stalder, and M. Seeley, “Air-Plasma Test Cell, Electron-Beam Source, and Measurements of Electron Density and Ozone Concentration,” DM1-6, 58th Annual Gaseous Electronics Conference, 16-20 Oct 2005, San Jose, CA, GEC05, 2005, Bulletin of the American Physical Society, Vol 50, No 7, p 16, 2005.

Vidmar, R., K. Stalder, and M. Seeley, “Experimental Details on Air-Plasma Measurements of Electron Density and Ozone Concentration,” SW33, 58th Annual Gaseous Electronics Conference, 16-20 Oct 2005, San Jose, CA, GEC05, 2005, Bulletin of the American Physical Society, Vol 50, No 7, p 55, 2005.

Vidmar, R., K. Stalder, and M. Seeley, “Electron Beam Produced Air Plasma: Measurements of Electron Density and Ozone Concentration,” Session 116-WIG-4, AIAA 2006-0791, p 10, 44th Aerospace Sciences Meeting and Exhibit, Reno, NV, 9-12 Jan, 2006.

Vidmar, R.J., K.R. Stalder, and M.V. Seeley, “Electron-Beam Produced Air Plasma: RF and Optical Diagnostics,” 33rd IEEE International Conference on Plasma Science, 4-8 June2006, Traverse City, Michigan, Poster 1P35, p 156, IEEE 06CH37759, ISBN 1-4244-0124-0, June 2006.

Vidmar, R.J., K.R. Stalder, and M.V. Seeley, “Electron-Beam Produced Air Plasma: Optical and Electrical Observations,” 33rd IEEE International Conference on Plasma Science, 4-8 June 2006, Traverse City, Michigan, Oral Presentation 3D6, p 219, IEEE 06CH37759, ISBN 1-4244-0124-0, June 2006.

Vidmar, R., K. Stalder, and M. Seeley, “Electron-Beam Produced Air Plasma: Optical Measurements of Beam Current,” Oral Presentation LW1-7, 59th Annual Gaseous Electronics Conference, 10-13 Oct 2006, Columbus, OH, GEC06, 2006,Bulletin of the American Physical Society, Vol 51,No 5, p 41, ISSN 0003-0503(200610)51;5;1-S, 2006.

Vidmar, R., K. Stalder, and M. Seeley, “Electron-Beam Produced Air Plasma: Optical and Electrical Diagnostics,” Poster SRP2-13, 59th Annual Gaseous Electronics Conference, 10-13 Oct 2006, Columbus, OH, GEC06, 2006, Bulletin of the American Physical Society, Vol 51,No 5, p 41,ISSN 0003-0503(200610)51;5;1-S, 2006.

Serdyuchenko, A. Y., M. V. Seeley, Q. J. Sinnott, and R. J. Vidmar, “Application of Tunable Diode Laser Spectroscopy for Time Resolved Measurements in Electron Beam Produced Plasma,” 2007 IEEE Pulsed Power and Plasma Science Conference, 17-22 June 2007,Albuquerque, New Mexico, Poster 2P10, June 2007.

Vidmar, R.J., A. Y. Serdyuchenko, M. V. Seeley, Q. J. Sinnott, and K. R. Stalder, “Electron-Beam Generated Air Plasma: Sensors to Quantify Beam Current and Electron Density,” 2007

IEEE Pulsed Power and Plasma Science Conference, 17-22 June 2007,Albuquerque, New Mexico, Poster 2P26, June 2007.

Serdyuchenko, A. Y., M. V. Seeley, Q. J. Sinnott, and R. J. Vidmar, "Chemical Composition of Electron Beam Produced Air Plasma by Means of Tunable Diode Laser Spectroscopy and Numerical Simulation," 2007 IEEE Pulsed Power and Plasma Science Conference, 17-22 June 2007, Albuquerque, New Mexico, Oral Presentation 3F1, June 2007.

Vidmar, R.J., A. Y. Serdyuchenko, M. V. Seeley, Q. J. Sinnott, and K. R. Stalder, "Electron-Beam Generated Air Plasma: Beam Current and Electron Density Distributions," 2007 IEEE Pulsed Power and Plasma Science Conference, 17-22 June 2007,Albuquerque, New Mexico, Oral Presentation 5B7, June 2007.

Vidmar, R., and K. Stalder, "Electrical and Optical Diagnostics of an Electron-Beam Generated Air Plasma," Oral Presentation PR1-53, 60th Annual Gaseous Electronics Conference, 2-5 Oct 2007, Arlington, VA, GEC07, 2007, Bulletin of the American Physical Society, Vol 52,No 8, p 48,ISSN 0003-0503(200710)52:8;1-L, 2007.

Vidmar, R., and K. Stalder, "Electron-Beam Generated Air Plasma: Electrical and Optical Diagnostic Details," Poster Presentation SRP1 16, 60th Annual Gaseous Electronics Conference, 2-5 Oct 2007, Arlington, VA, GEC07, 2007, Bulletin of the American Physical Society, Vol 52,No 8, p 58,ISSN 0003-0503(200710)52:8;1-L, 2007.

Vidmar, R., M. Seeley, A. Y. Serdyuchenko, and K. Stalder, "Electrical, RF, and Optical Diagnostics in E-Beam Excited Air Plasma," Session 191-PDL-7, AIAA 2008-1111, p 17, 46th Aerospace Sciences Meeting and Exhibit, Reno, NV, 7-10 Jan, 2008.

REFERENCES

Adamovich, I. V., "Control of Electron Recombination Rate and Electron Density in Optically-Pumped Non-Equilibrium Plasmas," J. Phys D: Appl. Phys., Vol 34, No 3, pp 319-325, 7 Feb, 2001.

Kluczynski, P., and O. Axner, “Theoretical description based on Fourier analysis of wavelength-modulation spectrometry in terms of analytical and background signals,” Appl. Opt. **38**, p 5803, 1999.

Macheret, S. O., M. N. Shneider, and R. B. Miles, “Modeling of Discharges Generated by Electron Beams in Dense Gases: Fountain and Thunderstorm Regimes,” Physics of Plasmas, Vol 8, No 5, pp 1518-1528, May, 2001.

Paul, J. B., L. Lapson, and J. G. Anderson, “Ultrasensitive absorption spectroscopy with a high-finesse optical cavity and off-axis alignment,” Appl. Opt. **40**, p 4904, 2001.

Stark, R. H., and K Schoenbach, "Electron Heating in Atmospheric Pressure Glow Discharges," J. Appl. Phys., Vol. 89, No. 7, pp 3568-3572, 1 April 2001.

Vidmar, R. J., Plasma Cloaking: Air Chemistry, Broadband Absorption, and Plasma Generation, NTIS, AFOSRTR900544, ADA2220440, p 88, 1990A.

Vidmar, R. J., "On the Use of Atmospheric Pressure Plasmas as Electromagnetic Reflectors and Absorbers," IEEE Transactions on Plasma Science, Vol 18, No 4, pp 733-741, Aug, 1990B.

Vidmar, R. J., and K. R. Stalder, “Air-Plasma Experimentation at the University of Nevada, Reno,” AIAA 2005-0791, p 12, Jan, 2005.

Vidmar, R., K. Stalder, and M. Seeley, “Electron Beam Produced Air Plasma: Measurements of Electron Density and Ozone Concentration,” Session 116-WIG-4, AIAA 2006-0791, p 10, 44th Aerospace Sciences Meeting and Exhibit, Reno, NV, 9-12 Jan, 2006.

Vidmar , R. J., and K. R. Stalder, Final Performance Report, AFOSR Grant FA95550-04-1-0015, pp 25, 29 Aug 2007

Vidmar, R. J., M. V. Seeley, A. Y. Serdyuchenko, and K. R. Stalder, “Electrical, RF, and Optical Diagnostics in E-Beam Excited Air,” AIAA 2008-1111, p 17, Jan, 2008.

Yu, L, C. O. Laux, DM Packan, and C. H. Kruger, "Direct-Current Glow Discharges in Atmospheric Pressure Air Plasma," J. Appl. Phys., Vol. 91, No. 5, pp 2678-2686, 1 March 2002.